New Letter of Intent to Jefferson Lab PAC 46

Beam-charge Asymmetries for Deeply Virtual Compton Scattering on the Neutron with CLAS12 at 11 GeV

S. Niccolai[1,2], E. Voutier[1], R. Dupré, M. Ehrhart, M. Guidal,
H.S. Ko, D. Marchand, C. Munoz Camacho, P. Chatagnon, R. Wang, S. Zhao
Institut de Physique Nucléaire d'Orsay, 91406 Orsay, France

Abstract

Measuring Deeply Virtual Compton Scattering on a neutron target is one of the necessary steps to deepen our understanding of the structure of the nucleon in terms of Generalized Parton Distributions (GPDs). DVCS on a neutron target allows to operate a flavor decomposition of the GPDs and plays a complementary role to DVCS on a transversely polarized proton target in the determination of the GPD E, the least known and least constrained GPD that enters Ji's angular momentum sum rule. To complete the experimental program of CLAS12 for DVCS on the neutron, we propose to measure beam-charge asymmetries for n-DVCS ($e^{\pm}d \rightarrow e'^{\pm}n\gamma(p)$) with the upgraded 11-GeV CEBAF positron/electron beam and the CLAS12 detector. For the detection of the recoil neutron, necessary to ensure the exclusivity of the reaction after having detected the scattered electron and the DVCS photon, we will use the Central Neutron Detector (CND) at backwards angles, and the forward calorimeters and time-of-flights at forward angles. Low-polar-angle photons will be detected in the Forward Tagger. Projections for the BCA on the 4-dimensional (Q^2, x_B, $-t$, ϕ) phase space, for 80 days of running on a deuterium target with the maximum luminosity for CLAS12 (10^{35}) are provided in this LOI. The sensitivity of this observable to the real part of E (and to the other GPDs) is evaluated via the simultaneous fit of all the projected nDVCS observables for CLAS12, with and without the proposed beam-charge asymmetry.

[1]co-spokesperson
[2]contact person, email: silvia@jlab.org

1 Introduction

It is well known that the fundamental particles which form hadronic matter are the quarks and the gluons, whose interactions are described by the Lagrangian of quantum chromodynamics (QCD). However, exact QCD-based calculations cannot yet be performed to explain all the properties of hadrons in terms of their constituents. Phenomenological functions need to be used to connect experimental observables with the inner dynamics of the constituents of the nucleon, the partons. Typical examples of such functions include form factors, parton densities, and distribution amplitudes. Generalized Parton Distributions (GPDs) are nowadays the object of an intense effort of research, in the perspective of understanding nucleon structure. The GPDs describe the correlations between the longitudinal momentum and transverse spatial position of the partons inside the nucleon, they give access to the contribution of the orbital momentum of the quarks to the nucleon, and they are sensitive to the correlated $q - \bar{q}$ components. The original articles and general reviews on GPDs and details of the formalism can be found in Refs. [1]-[7].

The nucleon GPDs are the structure functions which are accessed in the measurement of the exclusive leptoproduction of a photon (DVCS, which stands for deeply virtual Compton scattering) or of a meson on the nucleon, at sufficiently large Q^2, where Q^2 is the virtuality of the photon emitted by the initial lepton, for the reaction to happen at the quark level. Figure 1 illustrates the leading process for DVCS, also called the "handbag diagram". At leading-order QCD and at leading twist, considering only quark-helicity conserving quantities and the quark sector, the process is described by four GPDs, $H^q, \tilde{H}^q, E^q, \tilde{E}^q$, one for each quark flavor q, that account for the possible combinations of relative orientations of nucleon spin and quark helicity between the initial and final state. H and E do not depend on the quark helicity and are therefore called unpolarized GPDs while $\tilde{H}$ and $\tilde{E}$ depend on the quark helicity and are called polarized GPDs. H and $\tilde{H}$ conserve the spin of the nucleon, whereas E and $\tilde{E}$ correspond to a nucleon-spin flip.

The GPDs depend upon three variables, x, ξ and t: $x+\xi$ and $x-\xi$ are the longitudinal momentum fractions of the struck quark before and after scattering, respectively, and t is the squared four-momentum transfer between the initial and final nucleon (see caption of Fig. 1 for the definitions of these variables). The transverse component of t is the Fourier-conjugate variable of the transverse position of the struck parton in the nucleon. Among the three variables, x, ξ and t, which appear in the DVCS formalism, only ξ and t are experimentally accessible in these reactions.

The DVCS amplitude is proportional to combinations of integrals over x of the form:

$$\int_{-1}^{1} dx F(\mp x, \xi, t) \left[\frac{1}{x - \xi + i\epsilon} \pm \frac{1}{x + \xi - i\epsilon} \right], \tag{1}$$

where F represents one of the four GPDs. The top combination of the plus and minus signs applies to the quark-helicity independent, or unpolarized, GPDs (H, E), and the bottom combination of signs applies to the quark-helicity dependent, or polarized, GPDs $(\widetilde{H}, \widetilde{E})$. Each of these 4 integrals, which are called Compton Form Factors

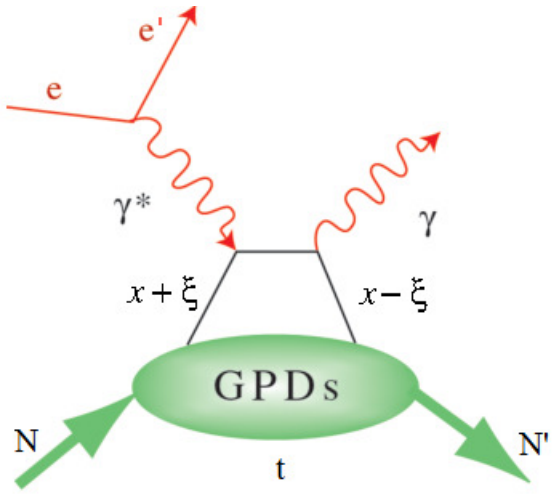

Figure 1: The handbag diagram for the DVCS process on the nucleon $eN \to e'N'\gamma'$. Here $x+\xi$ and $x-\xi$ are the longitudinal momentum fractions of the struck quark before and after scattering, respectively, and $t = (N - N')^2$ is the squared four-momentum transfer between the initial and final nucleons (or equivalently between the two photons). In the Bjorken limit, i.e. for $Q^2 \to \infty$ and $\nu \to \infty$ so that $x_B = \frac{Q^2}{2M\nu}$ is finite, ξ is proportional to the Bjorken scaling variable x_B ($\xi \simeq \frac{x_B}{2-x_B}$, where $x_B = \frac{Q^2}{2M\nu}$, M is the nucleon mass and ν is the difference between the energies of the initial and final electron in the lab frame).

(CFFs), can be decomposed into their real and imaginary parts, as

$$\Re\mathrm{e}\mathcal{F}(\xi,t) = \mathcal{P}\int_{-1}^{1} dx \left[\frac{1}{x-\xi} \mp \frac{1}{x+\xi}\right] F(x,\xi,t) \quad (2)$$

$$\Im\mathrm{m}\mathcal{F}(\xi,t) = -\pi[F(\xi,\xi,t) \mp F(-\xi,\xi,t)], \quad (3)$$

where $\mathcal{P}$ is Cauchy's principal value integral and the sign convention is the same as in Eq. 1. The information that can be extracted from the experimental data at a given (ξ, t) point depends on the observable involved. $\Re\mathrm{e}\mathcal{F}$ is accessed primarily measuring observables which are sensitive to the real part of the DVCS amplitude, such as double-spin asymmetries, beam-charge asymmetries or unpolarized cross sections. $\Im\mathrm{m}\mathcal{F}$ can be obtained measuring observables which are mainly sensitive to the imaginary part of the DVCS amplitude, such as single-spin asymmetries or cross-section differences. However, knowing the CFFs does not define the GPDs uniquely. A model input is necessary to deconvolute their x dependence.

The DVCS process is accompanied by the Bethe-Heitler (BH) process, in which the final-state real photon is radiated by the incoming or scattered electron and not by the nucleon itself. The BH process, which is not sensitive to the GPDs, is experimentally indistinguishable from DVCS and interferes with it at the amplitude level. However, considering that the nucleon form factors are well known at small t, the BH process is precisely calculable.

2 Physics motivation: neutron GPDs and flavor separation

The aim of this LOI is to complete the experimental program of CLAS12 for DVCS on the neutron. The importance of neutron targets in the DVCS phenomenology was clearly established in the pioneering Hall A experiment, where the polarized-beam cross section difference off a neutron, from a deuterium target, was measured [10].

Measuring neutron GPDs is complementary to measuring proton GPDs: quark-flavor separation of the GPDs becomes possible only if both the proton and neutron GPDs are measured. Since we can express

$$\mathcal{H}^p(\xi,t) = \frac{4}{9}\mathcal{H}^u(\xi,t) + \frac{1}{9}\mathcal{H}^d(\xi,t) \tag{4}$$

and

$$\mathcal{H}^n(\xi,t) = \frac{1}{9}\mathcal{H}^u(\xi,t) + \frac{4}{9}\mathcal{H}^d(\xi,t) \tag{5}$$

(and similarly for $\mathcal{E}$, $\tilde{\mathcal{H}}$ and $\tilde{\mathcal{E}}$), it immediately follows that

$$\mathcal{H}^u(\xi,t) = \frac{9}{15}(4\mathcal{H}^p(\xi,t) - \mathcal{H}^n(\xi,t)) \tag{6}$$

and

$$\mathcal{H}^d(\xi,t) = \frac{9}{15}(4\mathcal{H}^n(\xi,t) - \mathcal{H}^p(\xi,t)). \tag{7}$$

An extensive experimental program devoted to the measurement of GPDs using the DVCS channel on a proton target has been approved at Jefferson Lab, in particular with CLAS12. Single-spin asymmetries with polarized beam and/or linearly or transversely polarized proton targets, as well as unpolarized and polarized cross sections, will be measured with high precision and a vast kinematic coverage. If a similar program is performed on the neutron, the flavor separation of the various GPDs will be possible. An experiment to measure the beam-spin asymmetry for nDVCS, particularly sensitive to the GPD E_n, has already been approved [17]. The measurement of single- and double-spin asymmetries for nDVCS with a longitudinally polarized taget is also foreseen for the nearby future with CLAS12. The present LOI focuses on the extraction of one more observable, the beam-charge asymmetry. The next section will outline the CFFs to which this observable shows the most sensitivity.

2.1 Beam-charge asymmetry

The measurement of the cross-section asymmetry with respect to the beam charge, not taking into account the beam polarization,

$$A_{\rm C}(\phi) \equiv \frac{d\sigma^+ - d\sigma^-}{d\sigma^+ + d\sigma^-} = \frac{d\sigma^{\rm I}_{UU}}{d\sigma^{\rm BH}_{UU} + d\sigma^{\rm DVCS}_{UU}}, \tag{8}$$

is a way to single out the DVCS-BH interference term in the numerator. Using the BMK formalism [9], the Fourier expansion of $d\sigma^{\rm I}_{UU}$ is given by:

$$d\sigma^{\rm I}_{UU} = \frac{-K_{\rm I}}{\mathcal{P}_1(\phi)\,\mathcal{P}_2(\phi)} \sum_{n=0}^{3} c^{\rm I}_{n,\rm unp} \cos(n\phi), \tag{9}$$

The $d\sigma^{\rm DVCS}_{UU}$ term in the denominator has a $1/Q^2$ kinematic suppression. The dominant coefficient of BH term $d\sigma^{BH}_{UU}$ is $c^{\rm BH}_{0,\rm unp}$. However, the coefficient of the $\cos\phi$ term is also, often, not small.

The dominant coefficients, at leading twist, are $c^{\rm I}_{1,\rm unp}$ and $c^{\rm I}_{0,\rm unp}$:

$$c^{\rm I}_{1,\rm unp} \propto \Re{\rm e}[F_1\mathcal{H} + \xi(F_1+F_2)\widetilde{\mathcal{H}} - \frac{t}{4M^2}F_2\mathcal{E}], \tag{10}$$

$$c^{\rm I}_{0,\rm unp} \propto -\frac{\sqrt{-t}}{Q}\, c^{\rm I}_{1,\rm unp}. \tag{11}$$

Given the relative values of F_1 and F_2 in the case of a neutron target, the beam-charge asymmetry should be mainly sensitive to the real part of the GPD E_n, and, in a lesser way and depending on the kinematics, to the real part of $\widetilde{H}$.

3 Kinematics

An event generator for DVCS/BH and exclusive π^0 electroproduction on the neutron inside a deuterium target has been developed [13]. The DVCS amplitude is calculated according to the BKM formalism [9], while the GPDs have been taken from the standard CLAS DVCS generator [14]. The Fermi-motion distribution is calculated with the Paris potential [15].

The output of the event generator was fed through CLAS12 FASTMC, to simulate the acceptance and resolutions of electrons/positrons and photons in the Forward Detector. For the detection of photons with polar angles between 2.5^o and 4.5^o the Forward Tagger (FT) will be used [16]. Kinematic cuts to ensure the applicability of the GPD formalism ($Q^2 > 1$ GeV^2/c^2, $t > -1.2$ GeV^2/c^2, $W > 2$ GeV/c^2) have been applied. Figure 2 shows the coverage in Q^2, x_B and t that is obtained from the event generator for the n-DVCS/BH reaction, with an electron/positron beam energy of 11 GeV.

The three plots of Fig. 3 shows θ as a function of the energy (or the momentum) in the lab frame for the electron/positron, the photon, and the neutron. As expected, the scattered leptons and the photon are mostly emitted at forward angles, while the recoil neutron is going at backwards angles.

In the hypothesis of absence of Final State Interactions (FSI), the minimal requirement to ensure the exclusivity of the n-DVCS reaction from a deuterium target and to determine the final and initial state is to fully detect (PID, angles and momentum) the scattered electron/positron, the photon, and the neutron.

As shown in the previous section, the electron/positron and the DVCS photon will be emitted at small angles, and thus will be detected in the forward part of CLAS12

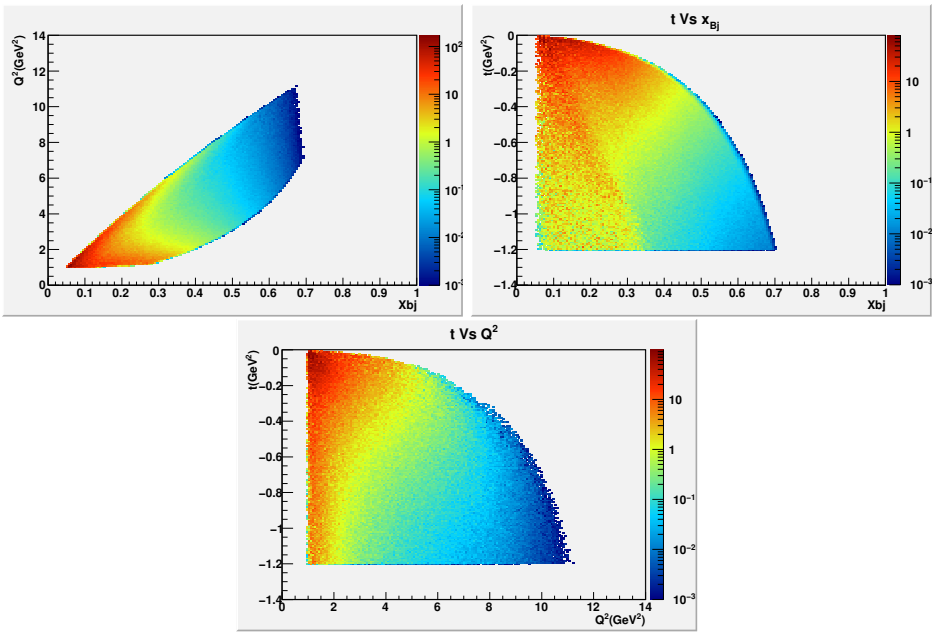

Figure 2: Distributions of kinematic variables for n-DVCS events. Forward-CLAS12 acceptance cuts and physics cuts are included. Top left: Q^2 as a function of x_B. Top right: t as a function of x_B. Bottom: t as a function of Q^2.

(with the photon either in the FEC or in the FT), while the neutron will be emitted predominantly (for $\sim$ 80% of the events) at $\theta > 40^o$ in the laboratory frame, with average momentum around 0.4 GeV/c. The CND and the CTOF will detect the high-θ neutrons, with a global efficiency of about 10-12%, while the remained of the neutrons will be detected in the forward scintillator-based detectors of CLAS12 (FEC, FTOF, PCAL).

4 Projections

The n-DVCS/BH final state will be reconstructed by detecting the scattered electron/positron and the DVCS/BH photon in the forward part of CLAS12 and the recoil neutron mostly in the CND, as very few neutrons are emitted in the forward direction with enough momentum to be detected in EC with appreciable efficiency. The expected number of reconstructed events for n-DVCS/BH has been calculated, as a function of the kinematics, with the event generator described in Section 3. The forward-CLAS12 fiducial cuts have been included, and an overall 10% neutron-detection efficiency for neutrons with $\theta > 40^o$ has been assumed. The detection efficiencies for electrons/positrons and photons efficiencies for the Forward Detector have been assumed to be 100%, within the fiducial cuts. The count-rate calculation has been done for a luminosity $L = 10^{35}$ cm^{-2}s^{-1} per nucleon (corresponding to roughly 60 nA

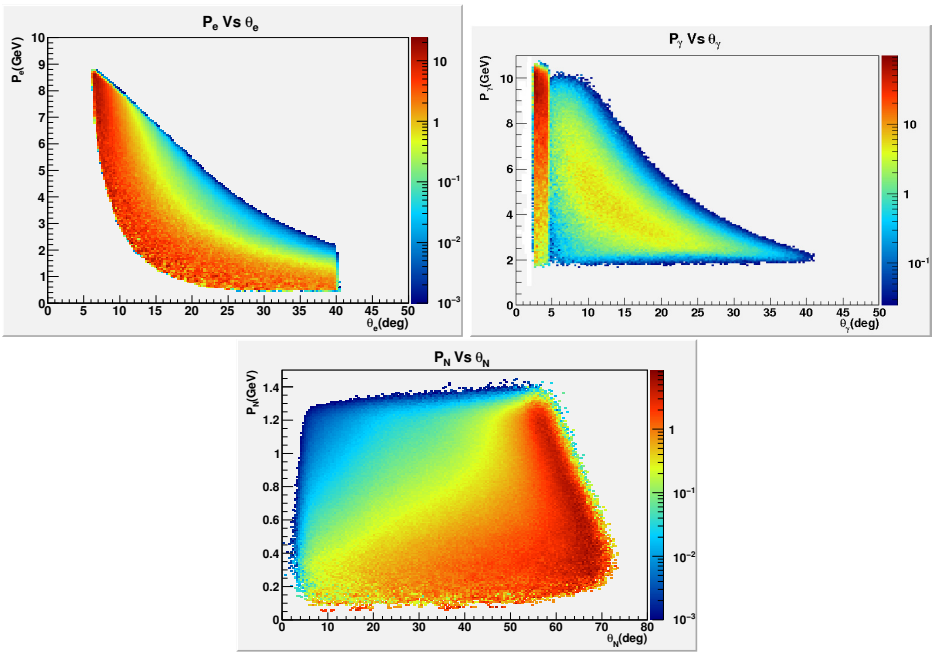

Figure 3: Energy as a function of polar angle, for n-DVCS events, for electrons/positrons (top left) and photons (top right). The bottom plot shows the momentum as a function of polar angle for nDVCS recoil neutrons. Forward-CLAS12 acceptance cuts and physics cuts are included.

of beam current) and for 80 days (40 with positron beam, 40 with electron beam) of running time. The following 4-dimensional grid of bins has been adopted here:

- 4 bins in Q^2 $[1, 2, 3.5, 5, 10$ GeV^2/c$^2]$
- 4 bins in $-t$ $[0, 0.2, 0.5, 0.8, 1.2$ GeV^2/c$^2]$
- 4 bins in x_B $[0.05, 0.15, 0.3, 0.45, 0.7]$
- 12 bins in ϕ, each 30^o wide.

The BCA is defined, for each 4-dimensional bin, as:

$$A = \frac{d^4\sigma^+ - d^4\sigma^-}{d^4\sigma^+ + d^4\sigma^-} = \frac{\frac{N^+}{Q^+} - \frac{N^-}{Q^-}}{\frac{N^+}{Q^+} + \frac{N^-}{Q^-}}, \tag{12}$$

where $Q^\pm$ is the integrated charge for events with positron and electron beam. Here we assumed $Q^+ = Q^-$.

The number of events $N^\pm$, for each 4-dimensional bin (Q^2, x_B, t and ϕ), has been computed as:

$$N = \frac{d\sigma}{dQ^2 dx_B dt d\phi} \cdot \Delta t \cdot \Delta Q^2 \cdot \Delta x_B \cdot \Delta\phi \cdot L \cdot T \cdot Acc \cdot Eff, \tag{13}$$

where $\frac{d\sigma}{dQ^2 dx_B dt d\phi}$ is the 4-fold differential cross section, T is the running time, L the luminosity, Acc is the bin-by-bin acceptance and Eff is the neutron-detection efficiency.

The statistical errors on the beam-charge asymmetries will then depend on the values of the BCA itself (A), through the formula:

$$\sigma_A = \frac{\sqrt{(1-A)^2}}{\sqrt{N}}. \tag{14}$$

Figure 4 shows the expected accuracy on the n-DVCS/BH beam-charge asymmetry, computed using the VGG model and assuming $J_u = .3$ and $J_d = .1$, for all 4-dimensional kinematic bins within the CLAS12 acceptance.

By summing on all the count rates obtained for the full grid of bins, we can have an estimate of the total expected count rate. Overall, roughly 25 million of n-DVCS/BH events are expected to be collected over the full kinematic range of interest, corresponding to an integrated rate of 4 Hz for the 80 days of running time.

5 Extraction of Compton Form Factors

The four sets of projected asymmetries (BSA from [17]), TSA and DSA from [18], and the beam-charge asymmetries shown in the top plot of Fig. 4, respectively) for all kinematic bins were processed using the fitting procedure developed by Michel Guidal to extract the Compton Form Factors of the neutron [8, 19]. It is based on

a local-fitting method at each given experimental $(Q^2, x_B, -t)$ kinematic point. In this framework there are eight real CFFs-related quantities (which, hereafter will be defined, for brevity, as "CFFs")

$$F_{Re}(\xi, t) = \Re\mathrm{e}\mathcal{F}(\xi, t) \tag{15}$$

$$F_{Im}(\xi, t) = -\frac{1}{\pi}\Im\mathrm{m}\mathcal{F}(\xi, t) = [F(\xi, \xi, t) \mp F(-\xi, \xi, t)]\,, \tag{16}$$

where the sign convention is the same as for Eq. 1. These CFFs are the almost-free[3] parameters, which are extracted from DVCS observables using the well-established DVCS+BH theoretical amplitude. The BH amplitude is calculated exactly while the DVCS one is taken at the QCD leading twist. The expression of these amplitudes can be found, for instance, in [11].

As there are eight CFF-related unknowns (four "real" CFFs, four "imaginary" ones) left as free parameters, including more observables, measured at the same kinematic points, will result in more tightly constrained fits and will increase the number and accuracy of CFFs extracted from them.

In the adopted version of the fitter code, $\tilde{E}_{Im}(n)$ is set to zero, as $\tilde{E}(n)$ is assumed to be purely real - it is parametrized in the VGG model by the pion pole $(1/(t - m_\pi^2))$. Thus, seven out of the eight real and imaginary parts of the CFFs are left as free parameters in the fit. A loose bound on the parameters is also applied, limiting them within the interval given by $\pm 5 \cdot \mathrm{VGG}$, where "VGG" stands for the prediction of the VGG model for the value of the CFF.

The results for the 7 neutron CFFs are shown in Figs. 5-11, as a function of $-t$, and for each bin in Q^2 and x_B. The blue points are the CFFs resulting from the fits of the four observables, while the red ones are the CFFs obtained fitting only the projections of the currently approved nDVCS experiments. The error bars reflect both the statistical precision of the fitted observables and their sensitivity to that particular CFFs. Only results for which the error bars are non zero, and therefore the fits have properly converged for that CFF, are included here.

The CFFs on which the proposed experiment will have the strongest impact is, as expected, $E_{Re}(n)$, for which the approved projections had hardly any sensitivity, and which will be extracted over basically the whole phase space thanks to the BCA. A considerable extension in the coverage will be also obtained for $\tilde{H}_{Re}(n)$. An overall improvement to the precision on the other CFFs, as well as an extension in the kinematic over which they can be extracted, will also be induced by the inclusion of the BCA in the nDVCS dataset to be fitted.

6 Systematic uncertainties

The goal of this experiment is to extract beam-charge asymmetries, which are ratios of absolutecross sections. In the ratio, several charge-independent terms terms, such

[3]The values of the CFFs are allowed to vary within ± 5 times the values predicted by the VGG model [11, 12].

Source of error	ΔBCA
Beam charge measurement	8%
π^0 contamination	5%
Acceptance	3%
Radiative corrections	1%
n-γ misidentification	5%
Total	11%

Table 1: Expected systematic uncertainties on the proposed measurement.

as acceptances, efficiencies, and radiative corrections, cancel out, in a first approximation. One of the main sources of systematic uncertainty for the proposed experiment will be the measurement of the beam charge, which here we assume to bring around 8% of systemastic uncertainties. The π^0 background estimation, which — due to the finite size of our bins — will depend on the accuracy of the description of the detector acceptance and efficiency and on the model used in the Monte-Carlo simulation to describe the $en\pi^0(p)$ reaction, will contribute with 5% to the overall systematic uncertainties. A similar contribution will come from neutron/photon misidentification. Due to its strong variations as a function ϕ and to the size of our bins, the acceptance will bring an additional 3% systematic error. A summary of the uncertainties induced by these various sources can be found in Table 1. The total systematic uncertainty will be therefore of the order of 11%, averaged over all the kinematics (the π^0-background uncertainty will actually vary depending on the bin).

7 Summary of experimental setup

We plan to measure beam-charge asymmetries for the DVCS/BH reaction on the neutron using a liquid deuterium target and an 11-GeV electron/positron beam. To detect the scattered electron and photon we will use the CLAS12 detector in its baseline configuration plus, at small angles, the forward electromagnetic calorimeter of the Forward Tagger. For the detection of the recoil neutron we will use the Central Neutron Detector and the CTOF at backwards angles, and the FEC, the PCAL, and FTOF at forward angles.

In order to match the acceptance of the two beam settings, we plan to run the positron-beam part of the experiment with opposite polarities for the CLAS12 torus and solenoid, with respect to the electron-beam part.

Taking into account the always-improving performance of the CLAS12 DAQ we hope that the trigger rate will be at the acceptable level at design luminosity $L = 10^{35}$ $\mathrm{s}^{-1}\mathrm{cm}^{-2}$ per nucleon. This will require positron beam currents of the order of 60 nA.

8 Conclusions

The strong sensitivity to the real part of the GPD E of the beam-charge asymmetry for DVCS on a neutron target makes the measurement of this observable very important for the experimental GPD program of Jefferson Lab. This sensitivity is maximal for values of x_B which are attainable only with a 11-GeV beam. Model predictions show that for kinematics that will be available with CLAS12 this asymmetry can be comparable in size to the one obtained for proton DVCS. Our GEANT4-based simulations show that a total of 80 days of beam time will be sufficient to collect good statistics on the BCAs for the nDVCS reaction over a wide phase space. The addition of this nDVCS observable to the ones that are already planned to be measured with CLAS12 will permit the model-independent extraction of the real parts of the E and $\tilde{H}$ GPDs of the neutron over the whole available phase space. Combining all the neutron GPDs to the proton ones, obtained from the fit of all the pDVCS observables that CLAS12 will measure, will ultimately allow the quark-flavor separation of all GPDs.

References

[1] D. Müller, D. Robaschik, B. Geyer, F.-M. Dittes, and J. Horejsi, Fortschr. Phys. **42** (1994) 101.

[2] X. Ji, Phys. Rev. Lett. **78** (1997) 610; Phys. Rev. D **55** (1997) 7114.

[3] A.V. Radyushkin, Phys. Lett. B **380** (1996) 417; Phys. Rev. D **56** (1997) 5524.

[4] J.C. Collins, L. Frankfurt and M. Strikman, Phys. Rev. D **56** (1997) 2982.

[5] K. Goeke, M. V. Polyakov and M. Vanderhaeghen, Prog. Part. Nucl. Phys. **47** (2001) 401.

[6] M. Diehl, Phys. Rept. **388** (2003) 41.

[7] A.V. Belitsky, A.V. Radyushkin, Phys. Rept. **418** (2005) 1.

[8] M. Guidal, Eur. Phys. J. A **37** (2008) 319.

[9] A.V. Belitsky, D. Müller, A. Kirchner, Nucl. Phys. B **629** (2002) 323-392.

[10] M. Mazouz et al., Phys. Rev. Lett. **99**, 242501 (2007).

[11] M. Vanderhaeghen, P.A.M. Guichon, M. Guidal, Phys. Rev. D **60**, 094017 (1999).

[12] M. Guidal, M. V. Polyakov, A. V. Radyushkin and M. Vanderhaeghen, Phys. Rev. D **72**, 054013 (2005).

[13] A. El Aloui and E. Voutier, private communication.

[14] H. Avakyan, private communication.

[15] M. Lacombe et al., Phys. Rev C **21** (1980) 861.

[16] M. Battaglieri, R. De Vita, S. Stepanyan, D. Weygand et al., "Meson Spectroscopy with low Q^2 electron scattering in CLAS12", proposal for Jefferson Lab PAC37.

[17] S. Niccolai, V. Kubarovsky, S. Pisano, and D. Sokhan, JLab experiment E12-11-003.

[18] S. Niccolai, A. Biselli, K. Keith, S. Pisano, and D. Sokhan, JLab experiment E12-06-109a.

[19] M. Guidal, H. Moutarde, M. Vanderhaeghen, Rep. Prog. Phys. **76**, 066202 (2013).

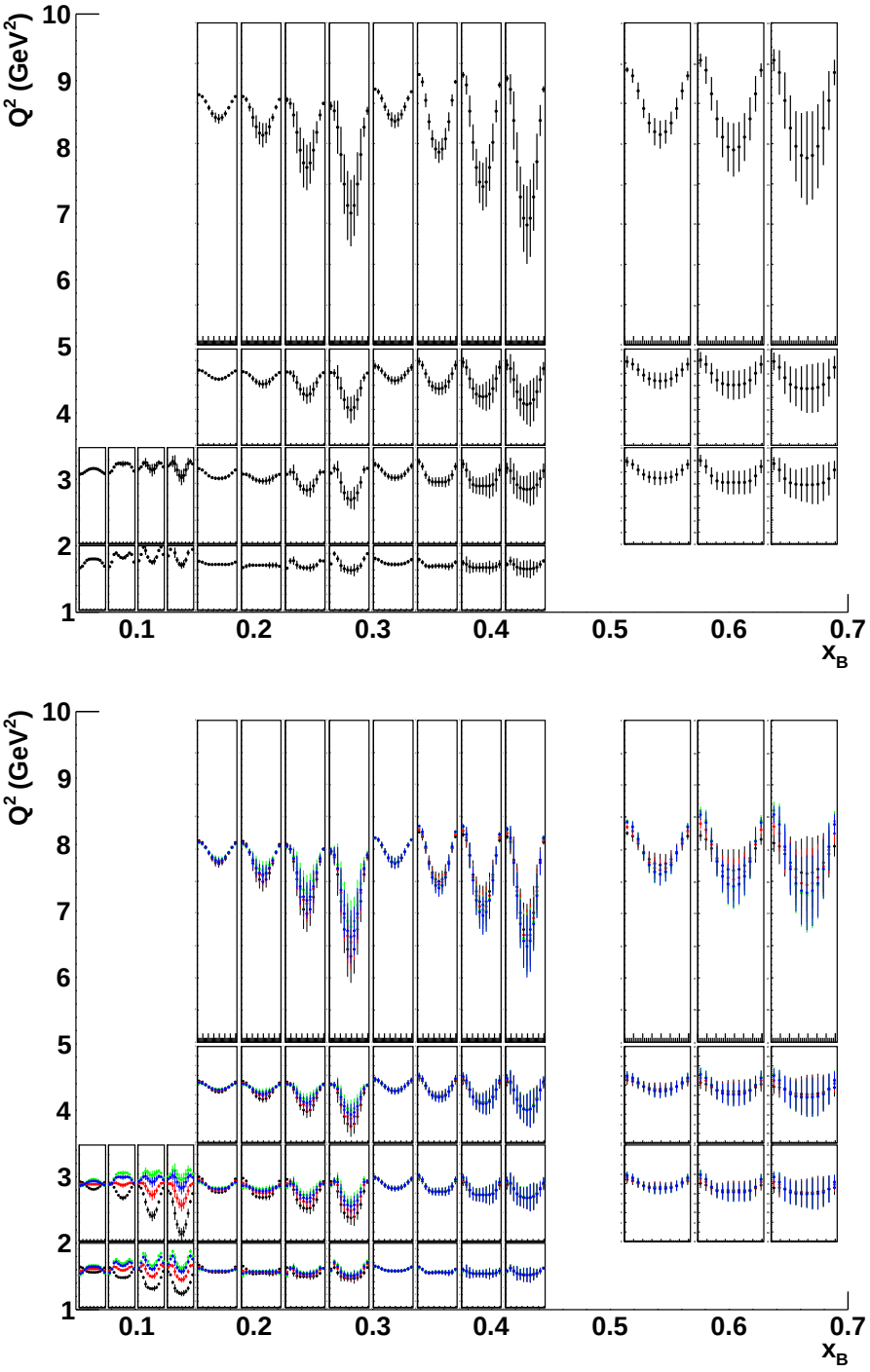

Figure 4: Beam-charge asymmetry for n-DVCS/BH as predicted by the VGG model. The top plot is obtained for $J_u = 0.3$ and $J_d = 0.1$. The for bottom plot compares different sets of values of J_u and J_d: 0.3/0.1 (black), 0.2/0.0 (red), 0.1/-0.1 (green), 0.3/-0.1 (blue)), plotted as a function of ϕ for all the covered bins in Q^2, x_B, and $-t$. The vertical axis scale ranges from -0.3 to 0.1 for the top plot and from -0.3 to 0.2 for the bottom plot. The error bars reflect the expected uncertainties for our CLAS12 experiment, corresponding to 80 hours of beam time at a luminosity of 10^{35} cm^{-2}s^{-1} per nucleon.

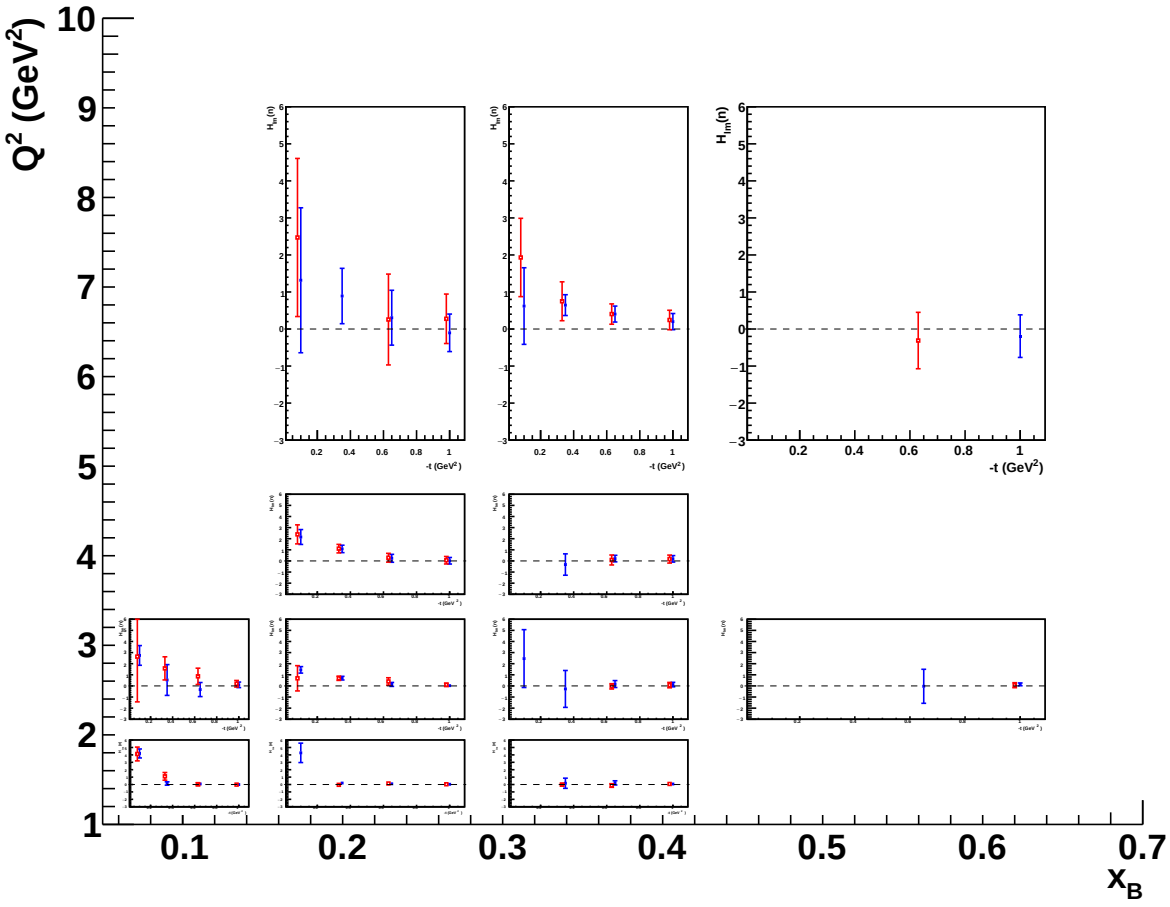

Figure 5: $H_{Im}(n)$ as a function of $-t$, for all bins in Q^2 and x_B. The blue points are the results of the fits including the proposed BCA, while the red ones do not include it.

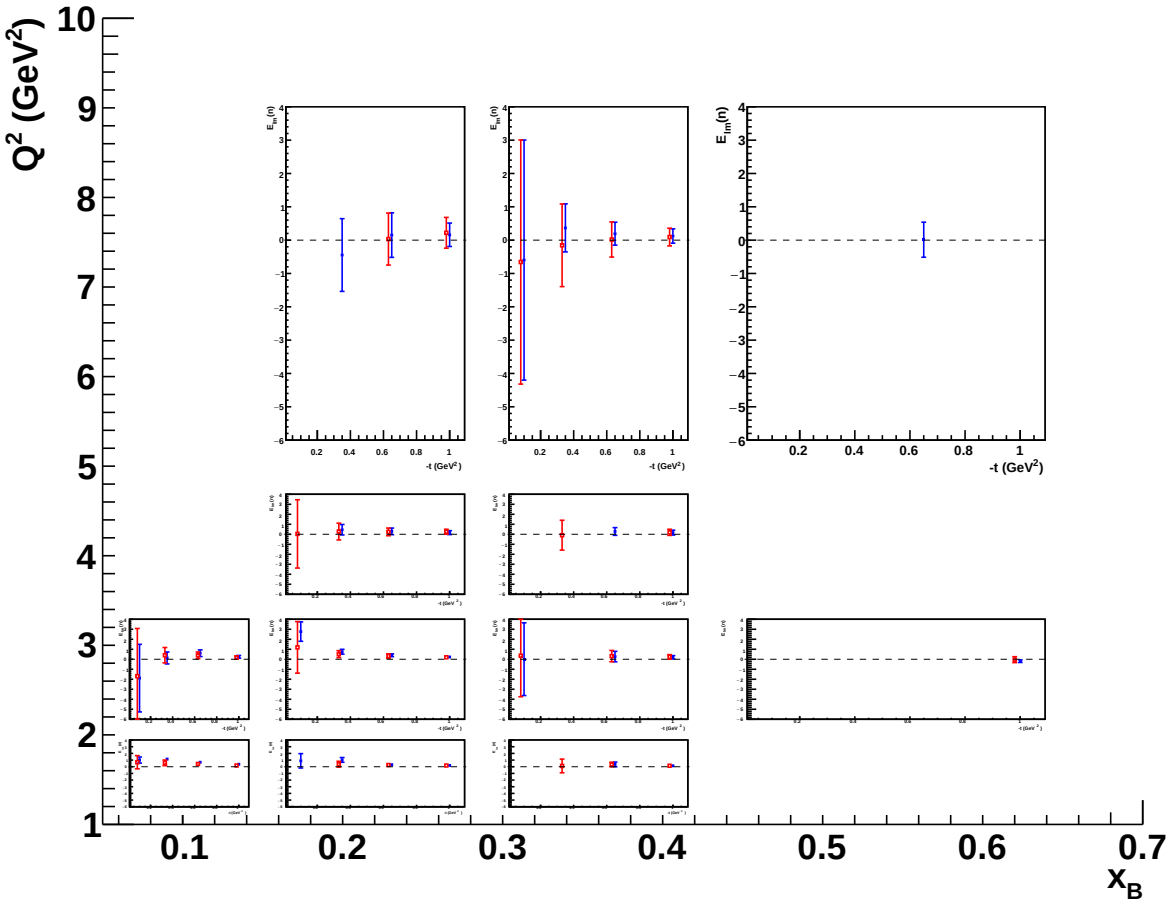

Figure 6: $E_{Im}(n)$ as a function of $-t$, for all bins in Q^2 and x_B. The blue points are the results of the fits including the proposed BCA, while the red ones do not include it.

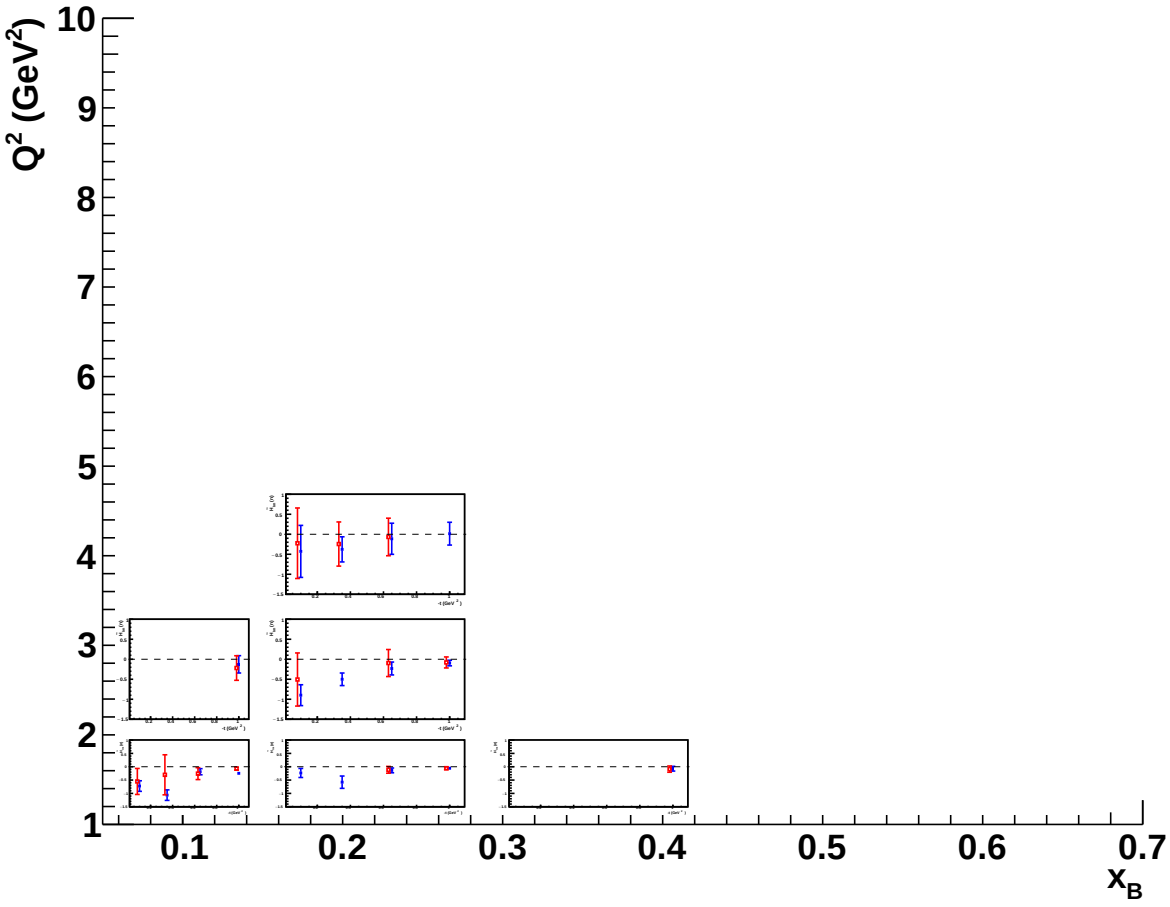

Figure 7: $\tilde{H}_{Im}(n)$ as a function of $-t$, for all bins in Q^2 and x_B. The blue points are the results of the fits including the proposed BCA, while the red ones do not include it.

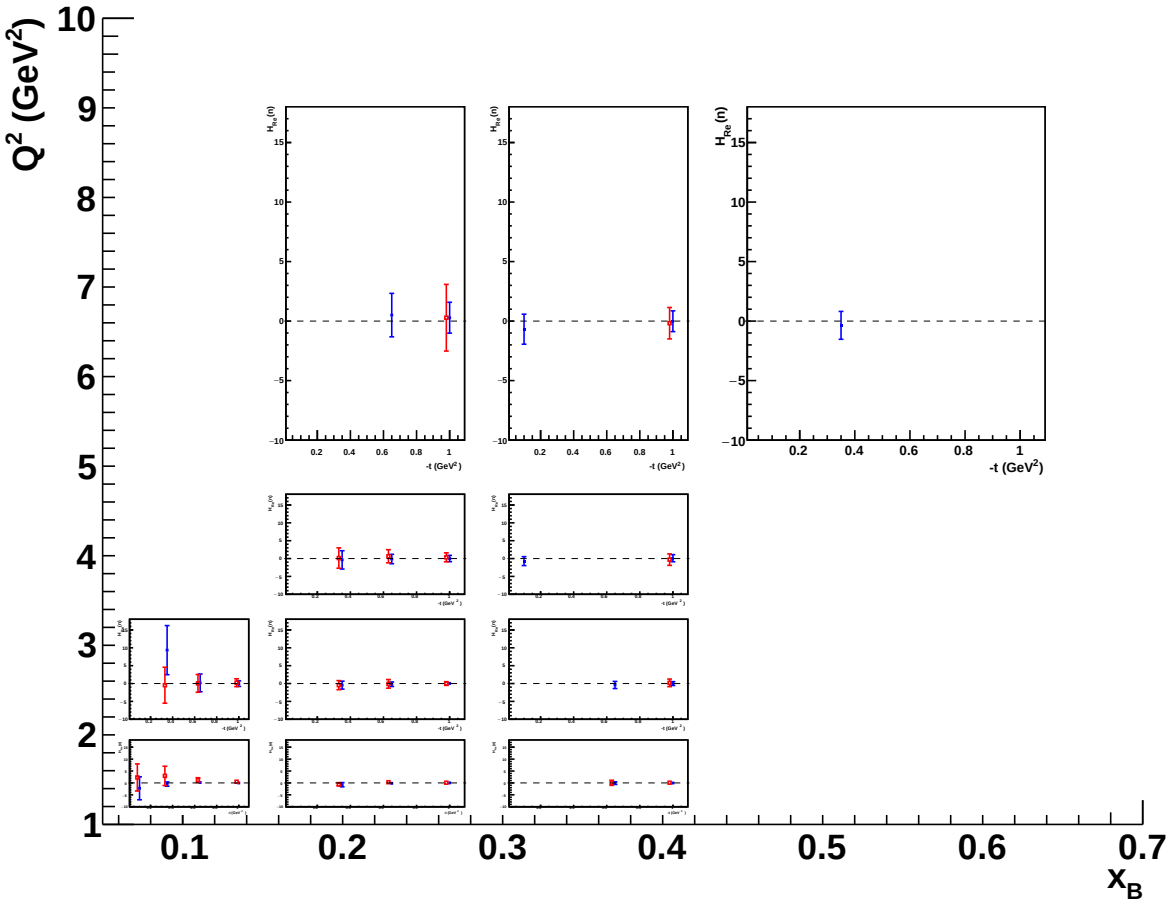

Figure 8: $H_{Re}(n)$ as a function of $-t$, for all bins in Q^2 and x_B. The blue points are the results of the fits including the proposed BCA, while the red ones do not include it.

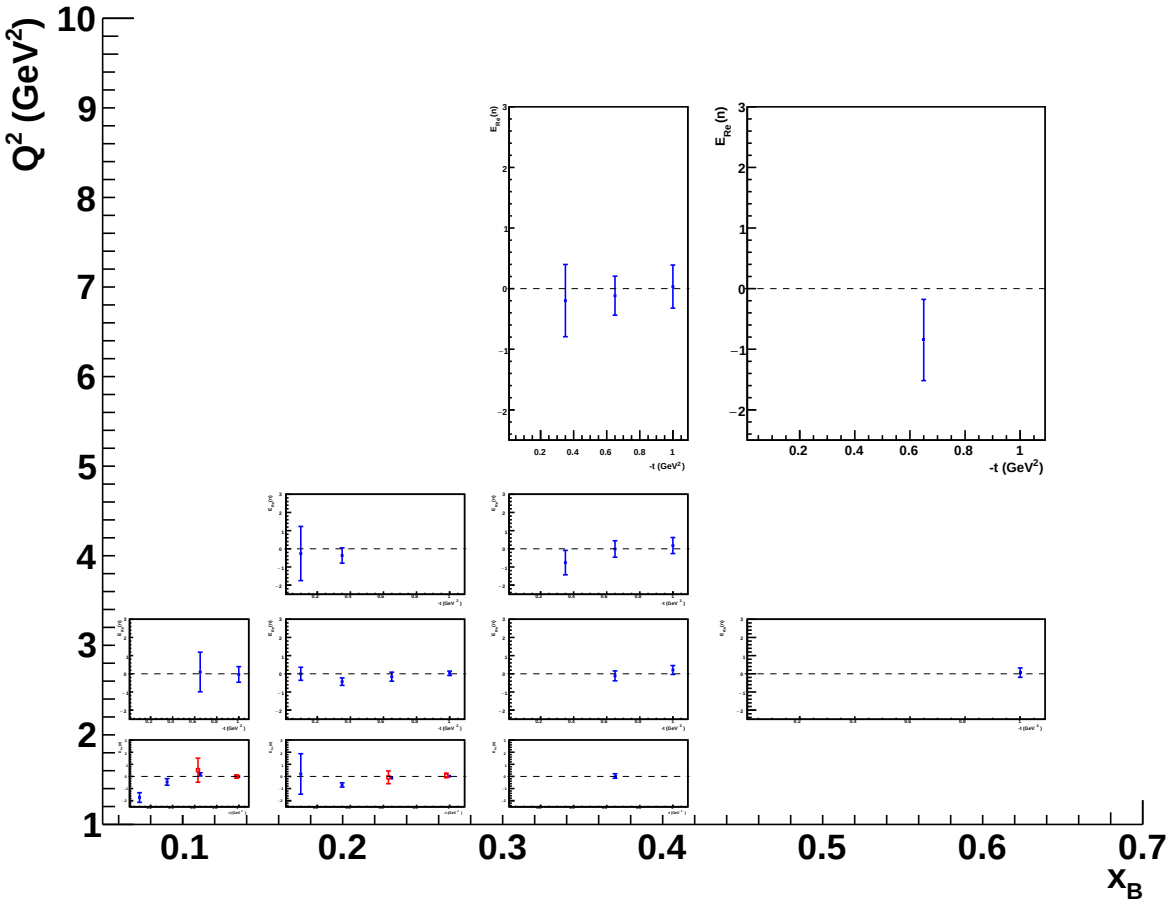

Figure 9: $E_{Re}(n)$ as a function of $-t$, for all bins in Q^2 and x_B. The blue points are the results of the fits including the proposed BCA, while the red ones do not include it.

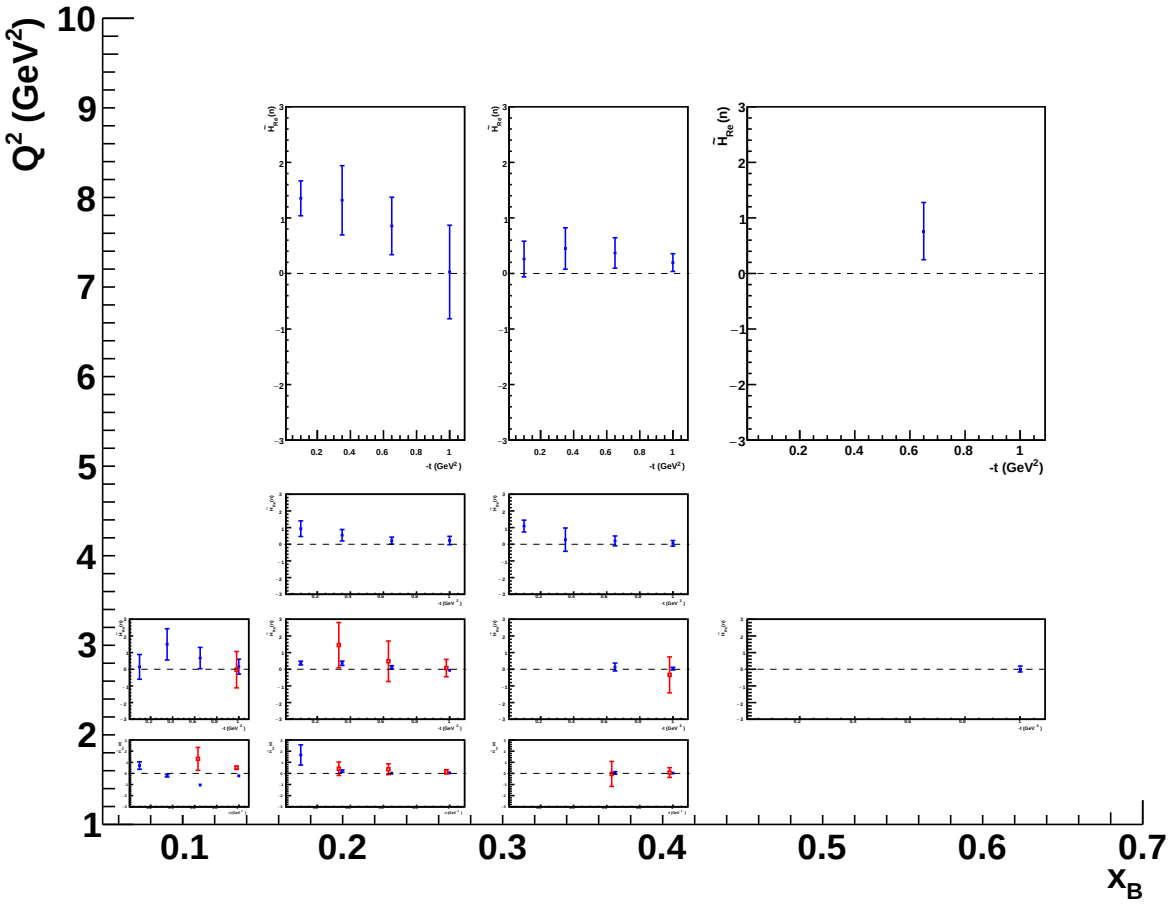

Figure 10: $\tilde{H}_{Re}(n)$ as a function of $-t$, for all bins in Q^2 and x_B. The blue points are the results of the fits including the proposed BCA, while the red ones do not include it.

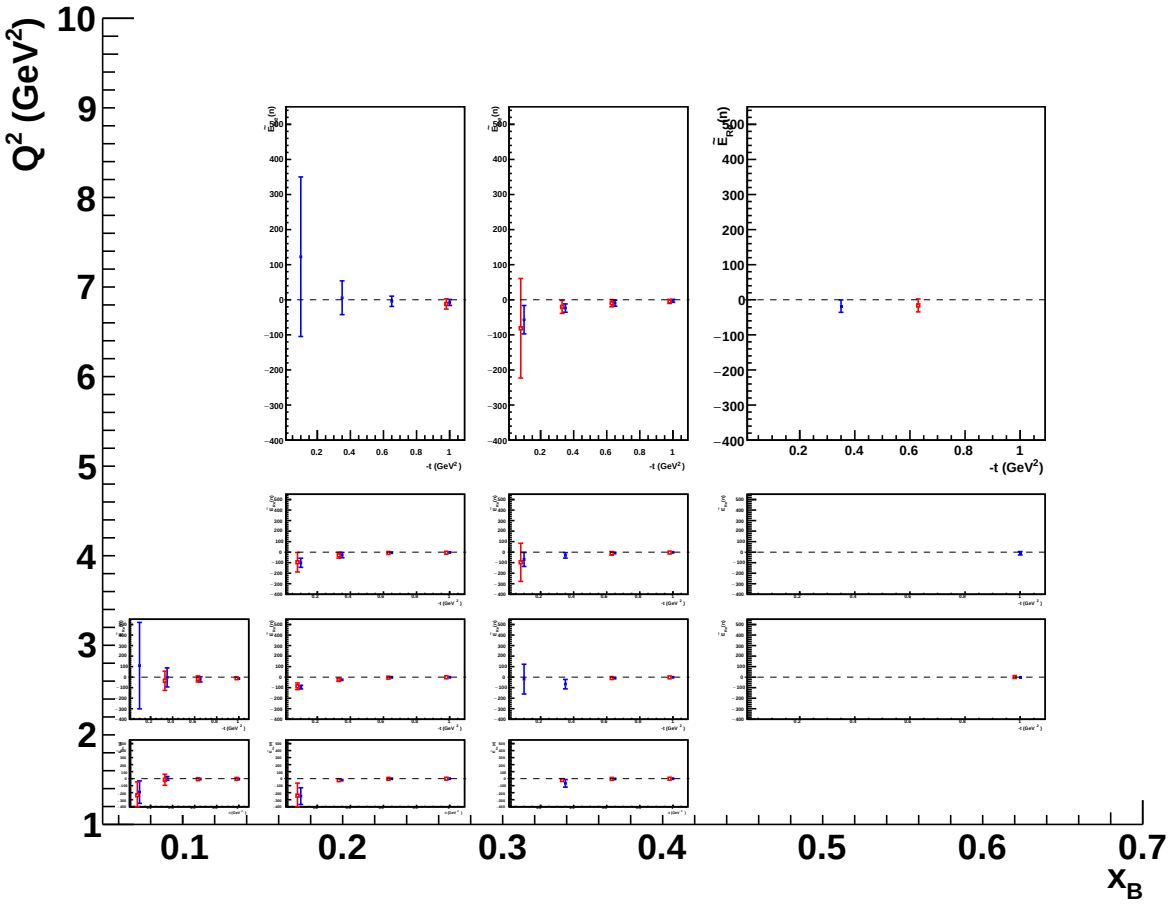

Figure 11: $\tilde{E}_{Re}(n)$ as a function of $-t$, for all bins in Q^2 and x_B. The blue points are the results of the fits including the proposed BCA, while the red ones do not include it.